JOURNAL OF MATERIALS SCIENCE 21 (1986) 4318–4326

Structure and properties of ion-nitrided stainless steels

K. OZBAYSAL, O. T. INAL*
Department of Metallurgy and Materials Engineering, New Mexico Institute of Mining and Technology, Socorro, New Mexico 87801, USA

The structure and properties of ion-nitrided layers on several stainless steels, 410 martensitic stainless steel, 430 ferritic stainless steel and 321 austenitic stainless steel, has been studied under varying process conditions with microhardness–depth correlations, optical microscopy and transmission electron microscopy. The process variables studied include time (2 to 10 h) and temperature (400 to 600° C). The highest case depth values and hardness levels were observed in martensitic stainless steels. The lowest case depths were observed in austenitic stainless steel. In general, the behaviour of matensitic and ferritic stainless steels were similar. All three steels showed increasing case depths and decreasing surface hardnesses with increasing ion-nitriding temperatures and times. Nitriding depth was found to be parabolic with ion nitriding time in all three steels at all ion-nitriding temperatures investigated, the nitriding reaction being faster in martensitic stainless steel than the others. Electron microscopy showed that almost no structural difference arises in the core of ferritic and austenitic stainless steels whereas recrystallization of the martensitic structure was observed in the core of martensitic steel following ion nitriding. Electron microscopy results also showed that ion nitriding produces platelets or disc-shaped precipitates on {0 0 1} matrix planes, coherent with the matrix. These platelets showed a striated morphology which is thought to be the result of the elastic strain in the matrix.

1. Introduction

The surface hardening of steels by nitriding has become an important commercial process in the past 50 years. This importance has grown from the fact that, through nitriding, very hard surface layers may be obtained without substantial modification of the bulk material properties. Although ammonia gas nitriding is by far the most common method used, the process of ion nitriding has recently become an industrial process [1–3].

Recent studies on ion-nitriding behaviour of speciality steels have indicated this process to be superior to the conventional nitriding processes in both core properties and the surface hardnesses achieved [4–8]. The structures of low-alloy commercial steels were observed by Inal and Robino [9, 10] with field ion and transmission electron microscope techniques. These observations showed the nucleation and growth of very small nitride precipitates, on {1 0 0} planes of ferrite, adjacent to the carbides that were produced in the tempering procedure.

Ozbaysal *et al.* [11] studied the structure and properties of ion-nitrided layers on tool steels. Their study showed that the iron–chromium carbides were converted to chromium nitrides in the regions close to the surface, within the nitrided case, whereas conversion was not complete at greater depths. This was attributed to the lower nitrogen activity at greater depths, from the nitrided surface.

One of the most attractive uses for plasma nitriding is in the treatment of the stainless steels. Because of their high chromium content, all stainless steels can be nitrided to some degree. Although nitriding adversely affects the corrosion resistance, it increases the surface hardness, provides a lower coefficient of friction and thus improves abrasion and fatigue resistance. These steels, used in applications where corrosion resistance is generally required, are assumed to be difficult to nitride. They normally require a pickling operation to remove the surface oxide film, which, if left on, would hinder nitrogen diffusion. The scope of the study presented was to delineate the ion-nitriding behaviour of various stainless steels.

2. Experimental procedure

The ion-nitriding system used in this study is the same as that used in our earlier investigations [11–13]. For all the experiments reported here, the total gas pressure was set at a constant value of 15 torr and the gas mixture was set at 0.25 + 0.008 volume fraction of nitrogen. The samples were discs 2.5 cm and 0.64 cm thick, the surfaces of which were ground to 600 grit silicon carbide. The compositions of the steels are given in Table I. Ferritic and austenitic stainless steels were in the annealed condition, whereas martensitic stainless steel was in the quenched and tempered condition, as discs, prior to ion nitriding, in accordance with the standard pre-nitriding procedures [1].

*Author to whom all correspondence should be addressed.

0022–2461/86 $03.00 + .12

TABLE I Composition (in wt %) of the steels used in this investigation

	C	Mn	Si	P	S	Cr	Ni	Other
410	0.15	1.00	1.00	0.040	0.030	11.50/13.50	–	
430	0.12	1.00	1.00	0.040	0.030	16.00/17.00	–	
321	0.08	2.00	1.00	0.045	0.030	17.50/19.00	9.00/12.00	Ti5 × C

The dependence of surface hardness and case depth of ferritic and martensitic steels were investigated by ion nitriding between 400 and 520° C, whereas a temperature range of 480 to 600° C was used for austenitic stainless steel treatments. Ion-nitriding times were varied between 2 and 10 h, at a constant partial pressure of nitrogen (25%).

Microhardness (VHN) measurements were used to determine the case depth as well as to aid in the characterization of case as a function of depth. For the microhardness–depth correlations, a minimum of three indentations were made at each depth. All microhardness measurements were conducted with a 200 g load. Surface hardness measurements were made after mechanical removal of the compound layer with 0.06 alumina.

Samples, which were subjected to microhardness testing, were sectioned, mounted cross-sectionally, and polished through 0.06 alumina. A composite of SiC powder and a low temperature setting resin was used for the specimen mounts to ensure edge retention during polishing. Samples observed in optical microscopy were etched using Vigella reagent [12].

Specimens for transmission electron microscopy were prepared by sectioning off the nitrided layer with a low speed saw and polishing by using standard twin-jet electro-polishing techniques. Specimens of the quenched and tempered materials and of the core samples were prepared in a similar manner. The quenched and tempered core and case of the nitrided samplers were examined in a Hitachi HU-200F transmission electron microscope operated at 200 kV.

3. Results and discussion

In the glow discharge nitriding procedures utilized in this study, an attempt was made to nitride common industrial stainless steels. After nitriding, the steels utilized contained a thin "compound layer" which was removed prior to hardness testing. During the initial part of the study, the effect of time and temperature on case depth was evaluated by nitriding with varying values of these parameters.

In general, martensitic (410) and ferritic (430) grades received larger case depths than austenitic (321) stainless steel. This behaviour can also be clearly seen in Fig. 1 in the hardness–depth plot for the samples treated at 520° C for 8 h. The martensitic steel showed a greater amount of hardening, while austenitic steel exhibited the lowest. The behaviour observed in martensitic and ferritic grades was similar, although the martensitic grade appears to have somewhat superior nitriding properties as indicated by the higher hardnesses achieved.

The dependence of case depth on time is shown in Figs 2 to 4 for martensitic, ferritic and austenitic grades, respectively. The case depth for all three steels is seen to increase linearly with the square root of time at each ion-nitriding temperature, as expected from the volume-diffusion controlled growth. Therefore, the rate-limiting step is volume diffusion of nitrogen. In general, the case depth increases with increasing temperature for the fixed treatment time because of the increased nitrogen diffusivity. Fig. 5 shows the case depths of all three steels as a function of square root of time. A comparison of the slopes of these curves, which are the reaction rate constants for the

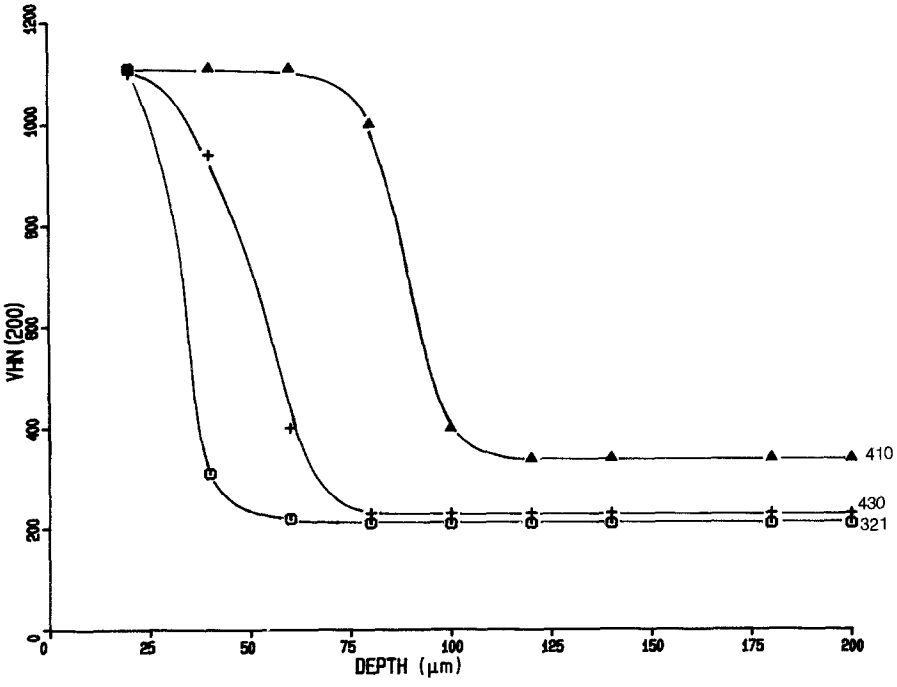

Figure 1 Hardness plotted against depth for the three steels investigated in this study.

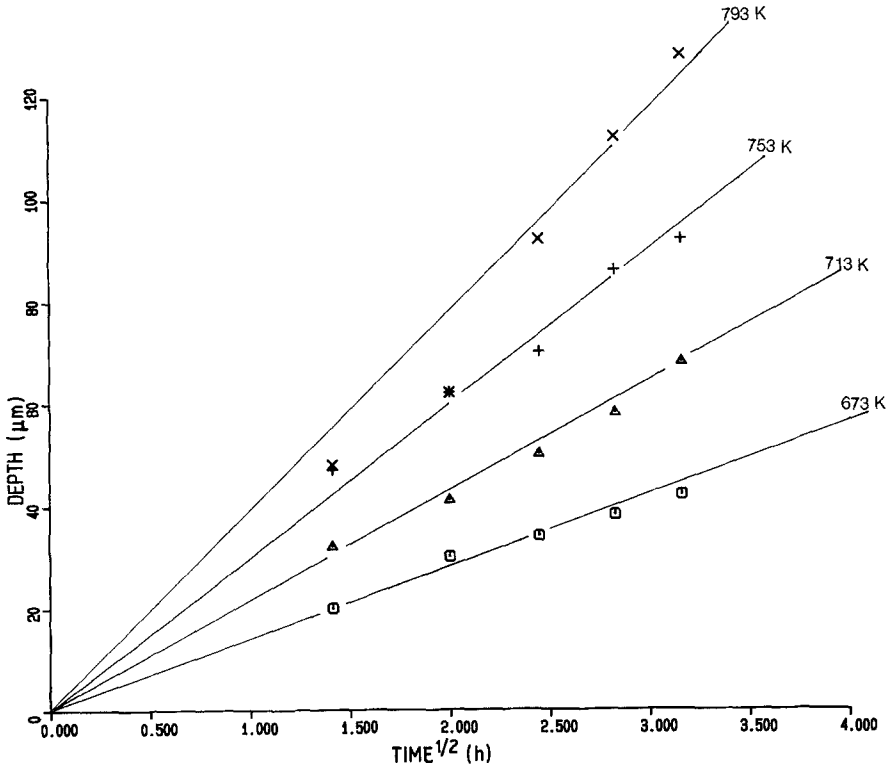

Figure 2 Case depth as a function of ion-nitriding time for 410 stainless steel.

steels investigated, shows that the nitriding reaction is fastest in the martensitic steel and slowest in the austenitic steel.

The difference in the observed diffusion behaviour of nitrogen arises from the structure dependency of nitrogen diffusion [14]. Activation energy for nitrogen diffusion is known to be higher in fcc austenite (47.3 kcal/mole), than it is in bcc ferrite (18.3 kcal/mole) [13, 15]. Therefore, austenitic stainless steel receives lower case depths, since the diffusivity of nitrogen is lower in this steel than the ferritic and martensitic grades. The slight superiority of martensitic grades over ferritic grades can again be explained with the aid of the structure sensitivity of interstitial diffusion [14]. Since ion-nitriding temperatures are relatively low, crystal defects play an important role in the diffusion of nitrogen. Small grain size and high dislocation density which exist in the martensitic structure probably were the short diffusion circuits for the diffusion of nitrogen, thus leading to the larger case depths observed in this steel.

Fig. 6 shows that the surface hardness of all three steels is a strong function of ion-nitriding temperature. In general, it is seen that the highest surface hardnesses were observed at low treatment temperatures for shorter ion-nitriding durations. This is thought to be an indication of precipitate size and density produced. There appear to be several complimentary factors which could contribute to this kind of behaviour. At the lowest ion-nitriding temperature the nitrogen uptake and the precipitate density are low and, therefore, the amount of hardening is also low.

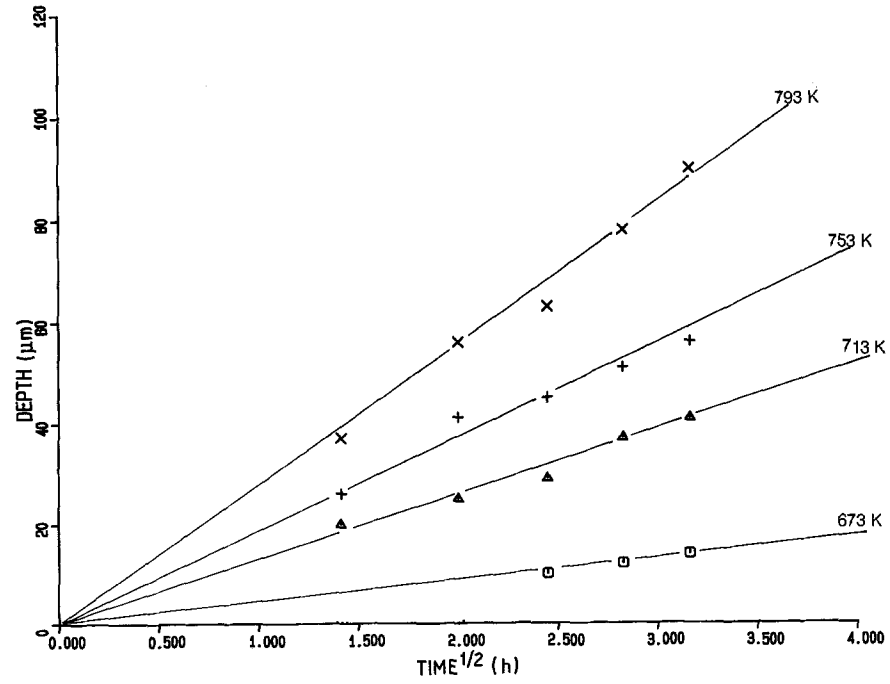

Figure 3 Case depth as a function of ion-nitriding time for 430 stainless steel.

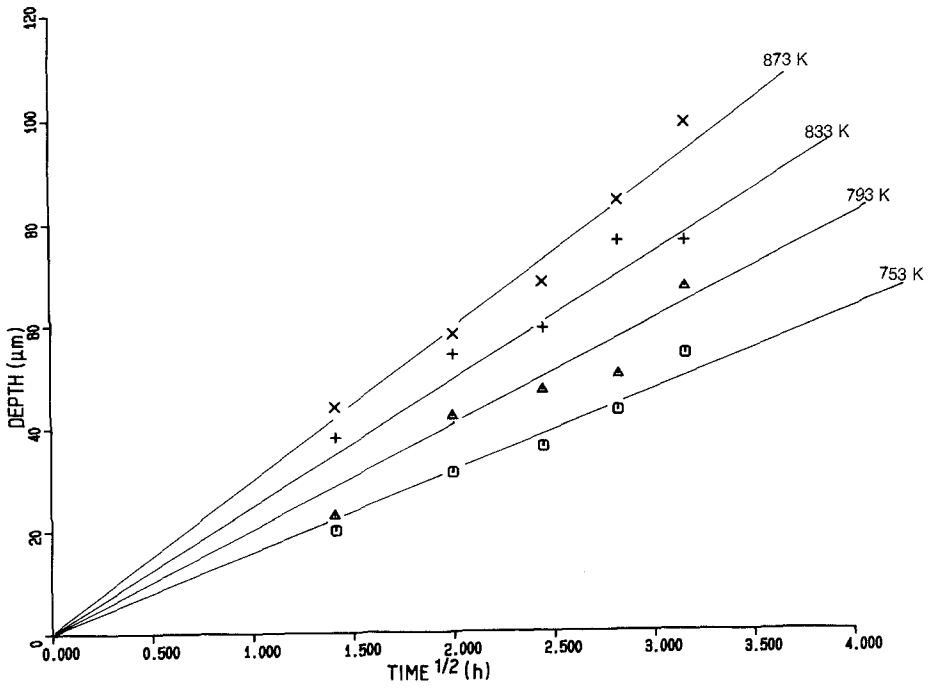

Figure 4 Case depth as a function of ion-nitriding time for 321 stainless steel.

At higher temperatures, and/or longer treatment times, precipitate growth becomes important. As has also been observed in many precipitation hardening alloys, in the present study, a maximum in surface hardness is achieved that corresponds to a particular ion-nitriding temperature and time. This hardness, in turn, is related to both precipitate density and precipitate size. Therefore, with regard to the nitriding of martensitic and ferritic stainless steels over a period of 6 h, a temperature range of 480° C produces an optimum nitride precipitate size and density. Also, in the case of martensitic stainless steel, matrix continues to temper and soften, thus reducing the hardness of both the case and the core. In this regard, the behaviour of austenitic stainless steel is still worth the mention. Having a higher activation energy for nitrogen diffusion, this steel has lower nitrogen diffusivity than the others. Since precipitation phenomena in nitriding systems are diffusion controlled, it can be expected that this steel receives a lower surface hardness than both in the martensitic and ferritic grades. However, Fig. 6 shows that austenitic grade receives higher hardnesses than the others, at 480° C, and the decrease in surface hardness with increasing ion-nitriding temperatures is less than that observed in the others. Austenitic stainless (321) steel contains an appreciable amount of titanium that precipitates as titanium carbide and thus the chromium content remains high enough to maintain its corrosion resistance. Since titanium nitride has a larger misfit with the matrix, it produces a larger strain in the matrix than does chromium nitride and, therefore, is more effective in hardening than chromium. Titanium nitride is also very stable in steels and does not lose its coherency with the matrix even at higher temperatures, after long exposure times [16]. This may account for the maintenance of

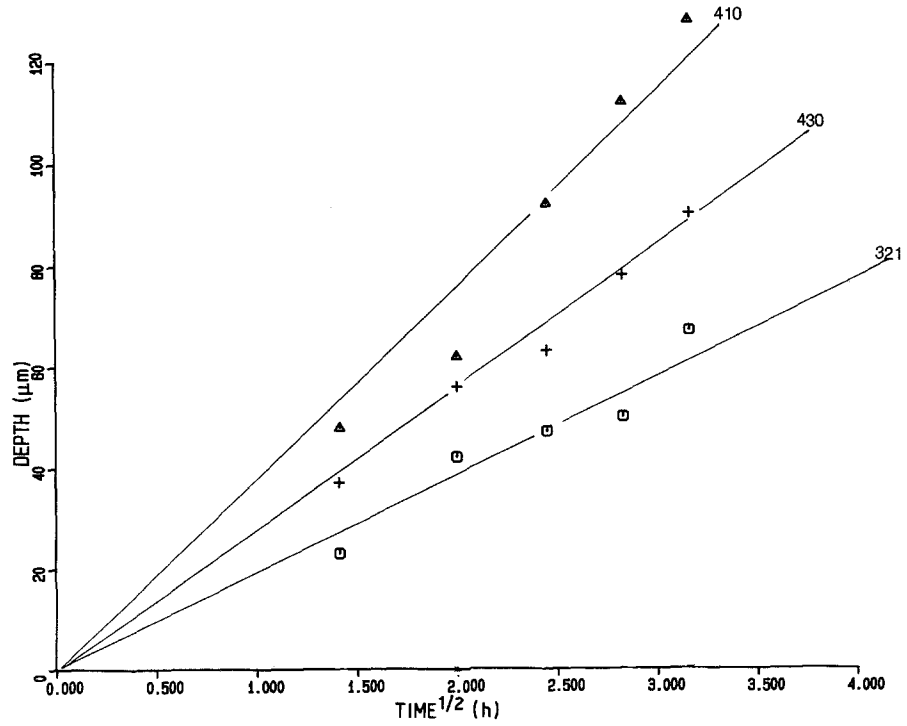

Figure 5 Case depth as a function of ion-nitriding time for three steels after ion nitriding at 520° C.

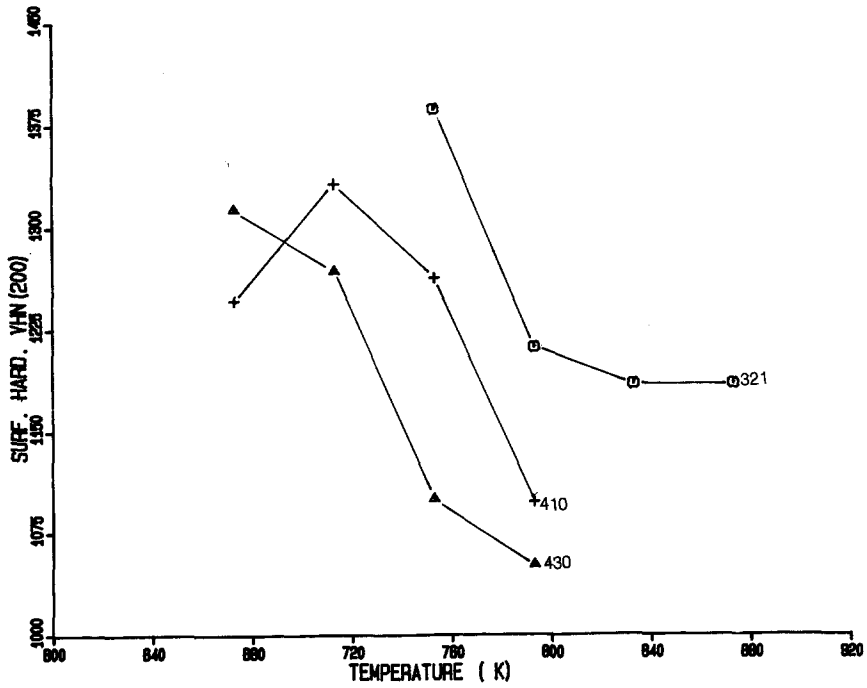

Figure 6 Surface hardness as a function of ion-nitriding temperature for three steels after ion nitriding for 6 h.

high surface hardness at high ion-nitriding temperatures in the austenitic stainless steel of this study.

Fig. 7 shows the optical micrographs of martensitic (410) grade in the quenched and tempered condition (Fig. 7a), ferritic grade (430) in the annealed condition (Fig. 7b), and austenitic grade (321) in the annealed condition (Fig. 7c), prior to ion nitriding. The absence of carbides from the grain boundaries in ferritic and austenitic steels and the annealing twins in austenitic stainless steel can be clearly seen (Figs 7b and c).

Figs 8a and b are the transmission electron micrographs of martensitic stainless steel in the quenched and tempered condition, prior to ion nitriding in Fig. 8a, and the core region after ion nitriding in Fig. 8b. The lath martensite structure expected of low carbon steels is visible in this steel. The original martensite laths, which have a high dislocation density and small grain size, can account for the high diffusivity of nitrogen in this steel. The microstructure has begun to recover and recrystallization is clear in some areas (Fig. 8b). This is the primary cause of softening of martensitic steel following ion nitriding, as mentioned earlier.

Figs 9a and b show the structure of ferritic steel in the annealed condition, prior to ion nitriding (Fig. 9a), and the core region after ion nitriding (Fig. 9b). There appears almost no structural change, after ion nitriding, in the core region. Since this steel does not undergo

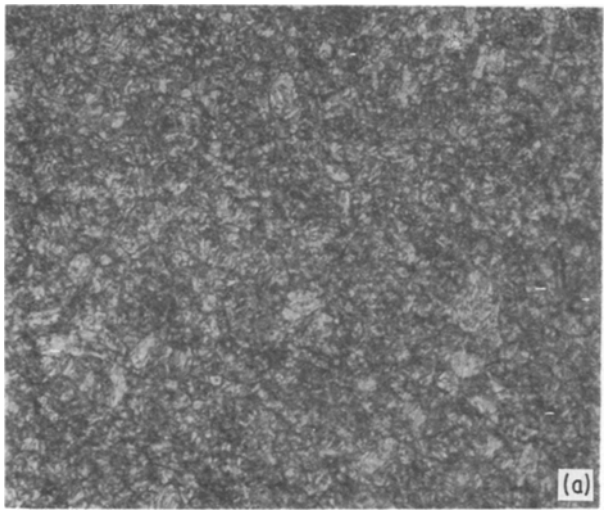

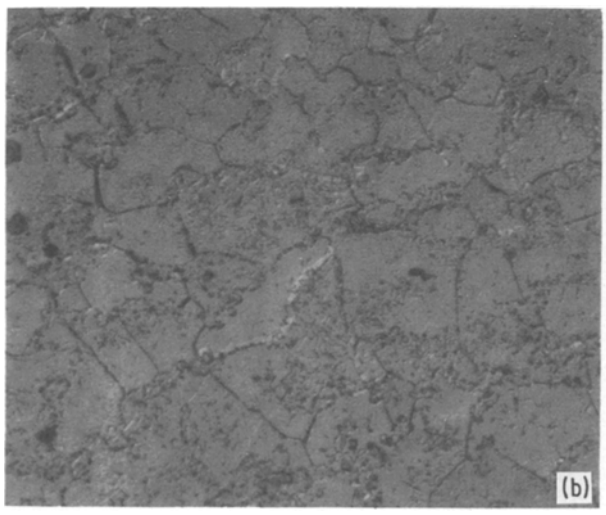

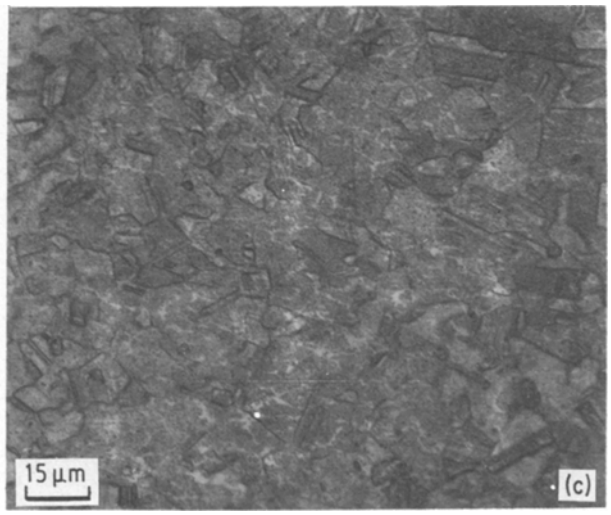

Figure 7 Optical micrographs of (a) 410, (b) 430 and (c) 321 prior to ion nitriding.

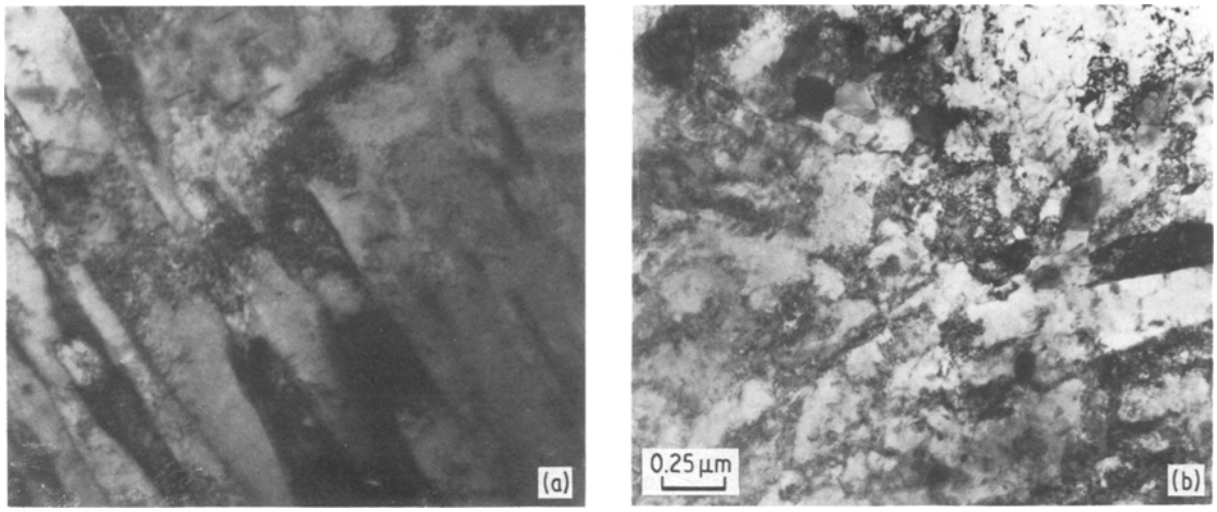

Figure 8 Transmission electron micrographs of 410 stainless steel in (a) the quenched and tempered condition and (b) the core region, after ion nitriding at 520° C for 10 h.

a phase transformation upon heating or cooling, this is to be expected. The same observations apply to the austenitic grade shown in Fig. 10. Fig. 10a is representative of the structure prior to ion nitriding, in the annealed condition. Fig. 10b shows the core region after ion nitriding. No structural change is visible after ion nitriding since this steel, like the ferritic grade, does not undergo a phase transformation within the ion-nitriding temperatures investigated. Nevertheless, the absence of carbides on the grain and twin boundaries in austenitic stainless steel and on the grain boundaries in ferritic stainless steel is obvious (in Figs 10b and 9b).

The microstructure of the case of nitrided martensitic (410) grade, approximately 50 to 60 μm below the surface, is shown in Fig. 11a. No regions of clear ferrite are seen, but elastic strain contrast doublets are visible; the latter is possibly due to the presence of small coherent nitride precipitates. The precipitates themselves are too small to resolve but the contrast produced by their strain fields is clearly visible. Further, dissolution of the carbides is indicated by the fact that no carbides are visible in Fig. 11a. As mentioned previously, the structure is seen to be made up of a fine dispersion of precipitates, the presence of which is resolvable but the exact shape of which is not. A slight modulation in the morphology is seen in the direction indicated by the arrow in Fig. 11a. The selected-area diffraction pattern corresponding to the area shown in Fig. 11a, but slightly larger, is shown in Fig. 11b. The pattern is a (0 0 1) matrix plane ([0 0 1] matrix direction is parallel to the beam) and has been rotated into proper coincidence with that of Fig. 11a. Streaking is observed in the $\langle 1\,0\,0 \rangle$ directions in the pattern, indicating that the precipitation has occurred as thin platelets on $\{1\,0\,0\}$ matrix planes. Also, the modulation direction in the bright-field image is coincident with the streaking in the pattern. No quantitative information is available on the composition of the precipitates but they are assumed to be chromium nitrides due to the composition of this steel (listed in Table I).

An electron micrograph of the case of nitrided ferritic grade is shown in Fig. 12a. Modulated elastic strain contrast is visible in the bright-field image, moving from the bottom to the top, as indicated by the arrow. The selected-area diffraction pattern obtained from the same area is shown in Fig. 12b. The foil orientation is again (0 0 1) and very pronounced streaks are observed in the $\langle 1\,0\,0 \rangle$ directions,

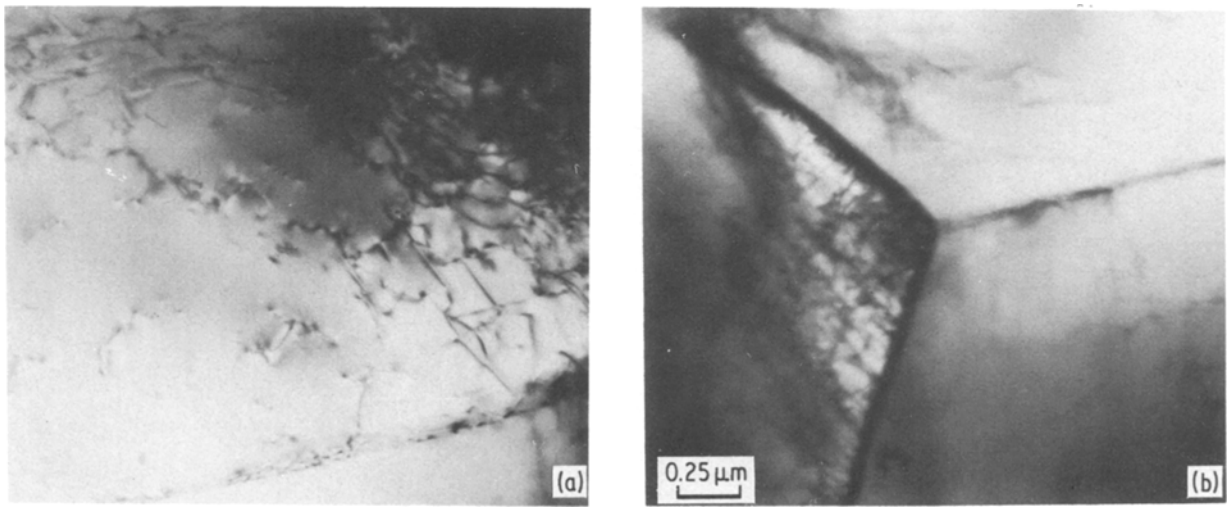

Figure 9 Transmission electron micrographs of 430 stainless steel in (a) the annealed condition and (b) the core region, after ion nitriding at 520° C for 10 h.

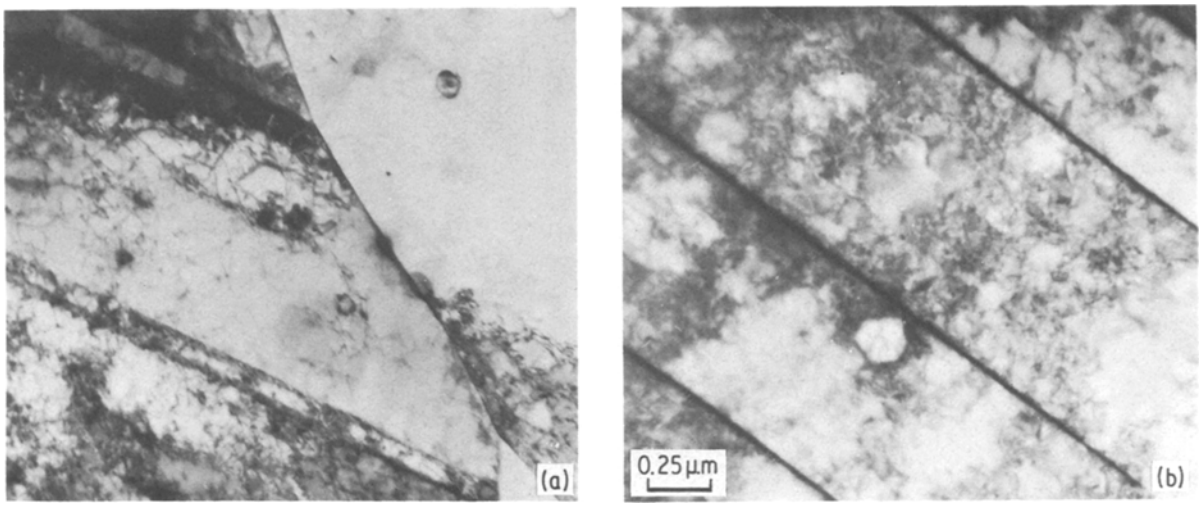

Figure 10 Transmission electron micrographs of 321 stainless steel in (a) the annealed condition and (b) the core region, after ion nitriding at 600° C for 10 h.

implying that the precipitation has occurred in ⟨1 0 0⟩ directions of matrix planes.

A bright-field image of the nitrided case of austenitic steel is given in Fig. 13a. This steel, as well as the other steels, shows the elastic strain contrast in the case region after ion nitriding. The modulated structure is again assumed to be due to the presence of small coherent precipitates, visible in Fig. 13a. The selected-area diffraction pattern obtained from the area shown in Fig. 13a is given in Fig. 13b, which corresponds to the (0 $\bar{1}$ 3) f c c matrix plane.

4. Conclusion

Two different types of nitriding behaviour were observed in this study. The first, exhibited by the martensitic (b c t) and ferritic (b c c) stainless steels, is characterized by faster formation of the diffusion layer that advances progressively into the core with time. The second type, exhibited by the austenitic stainless steel (f c c), is characterized by comparatively slower formation of the diffusion layer. This behaviour is attributed to the difference in activation energies for nitrogen diffusion in these steels. This may probably contribute to the difference in the observed diffusion results (case depths) for steels which have b c c and b c t (which is a distorted b c c) structures when compared with the austenitic (f c c) stainless steel.

The presence of titanium in the austenitic stainless steel may also be a contributing factor to the lower case depths observed. Titanium displays a strong affinity to nitrogen when compared with chromium [13]. It is, therefore, reasonable to assume that titanium nitride is the precipitating phase along with chromium nitride. This, in turn, could lead to faster consumption of nitrogen during nitriding. Thus, the slower reaction rates observed in austenitic stainless steel may be attributed to both its structure and the presence of titanium in its composition.

Electron microscopy results showed that nitriding produces several characteristics which are common to all steels. The nitride precipitates form as platelets or discs on {0 0 1} matrix planes. These precipitates are responsible for the streaking observed in the diffraction patterns and, in the case of martensitic and ferritic

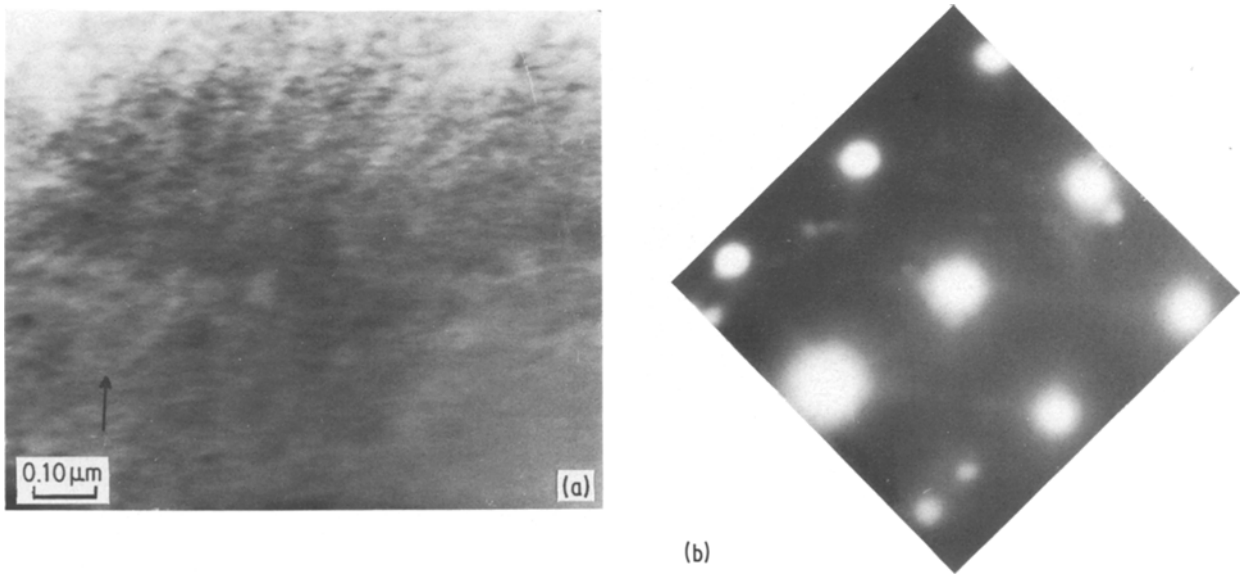

Figure 11 (a) Bright-field image of nitrided case of 410 steel after ion nitriding at 520° C for 10 h, and (b) the selected-area diffraction pattern of the corresponding area.

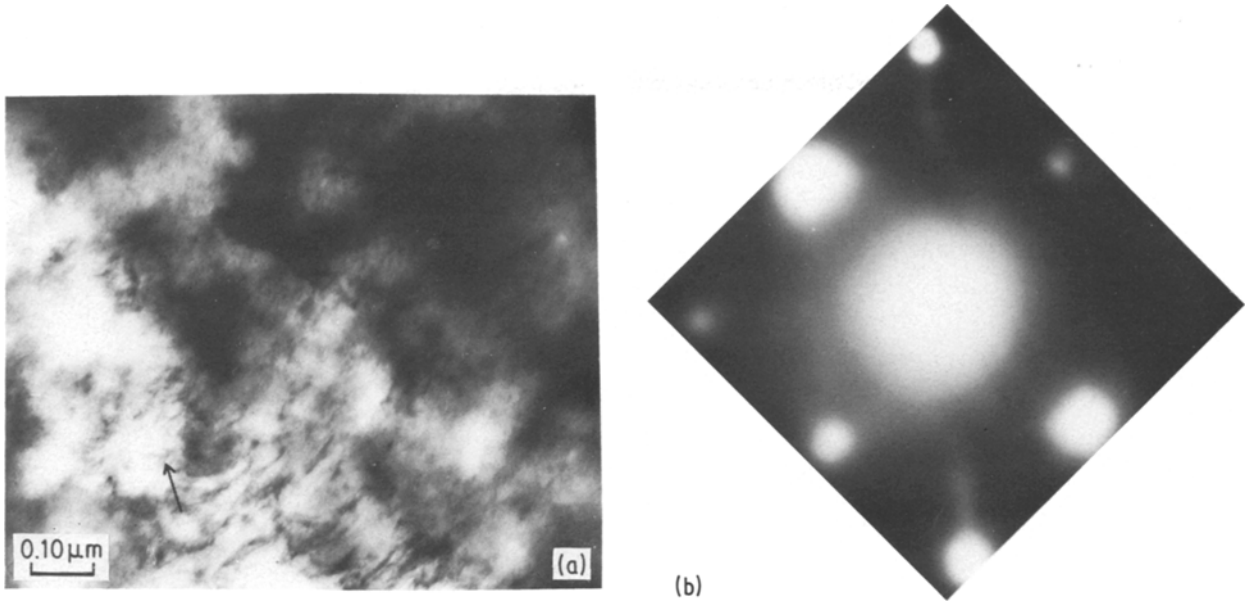

Figure 12 (a) Bright-field image of nitrided case of 430 steel after ion nitriding at 520° C for 10 h and (b) the selected-area diffraction pattern of the corresponding area.

grades, there are areas on the streaks of higher intensity. The surface hardness has been shown to increase dramatically after nitriding and this can allow for the design of components which can operate under more severe conditions. Although nitriding increases the surface hardness and wear resistance of stainless steels, it decreases the general corrosion resistance by combining surface chromium with nitrogen and depleting the amount needed for passive film formation [1]. Consequently, nitriding is not recommended for applications in which corrosion resistance is of major importance.

In spite of this, 410 and 422 types of nitrided stainless steels have successfully been used in steam turbine power generating equipment. Nitrided type 321 has also been used in the food industry and is also used to replace type 302 motor shaft [1]. Therefore, the desire for improved resistance to galling and spalling, as well as general wear resistance, may make ion nitriding a suitable choice for the surface treatment of these stainless steels.

Several conclusions can be derived from the results of this study.

1. Several trends are apparent:

(a) the surface hardness is a function of nitriding temperature,

(b) the diffusion layer increases parabolically with time in all three steels, suggesting that the process is volume-diffusion controlled.

2. The nitriding response is a strong function of the structure as well as composition. In this regard, the case depth was highest in martensitic steel closely followed by ferritic steel. Austenitic steel showed a far lower case depth following ion nitriding.

3. The surface hardness is maximum at treatment temperatures of around 440° C for martensitic steel and 480° C for austenitic steel.

4. No structural change in the core region of ferritic and austenitic stainless steels occurs after ion nitriding, whereas evidence of tempering of the core is seen in the microstructure of martensitic stainless steel.

5. The nitride precipitates can be characterized as

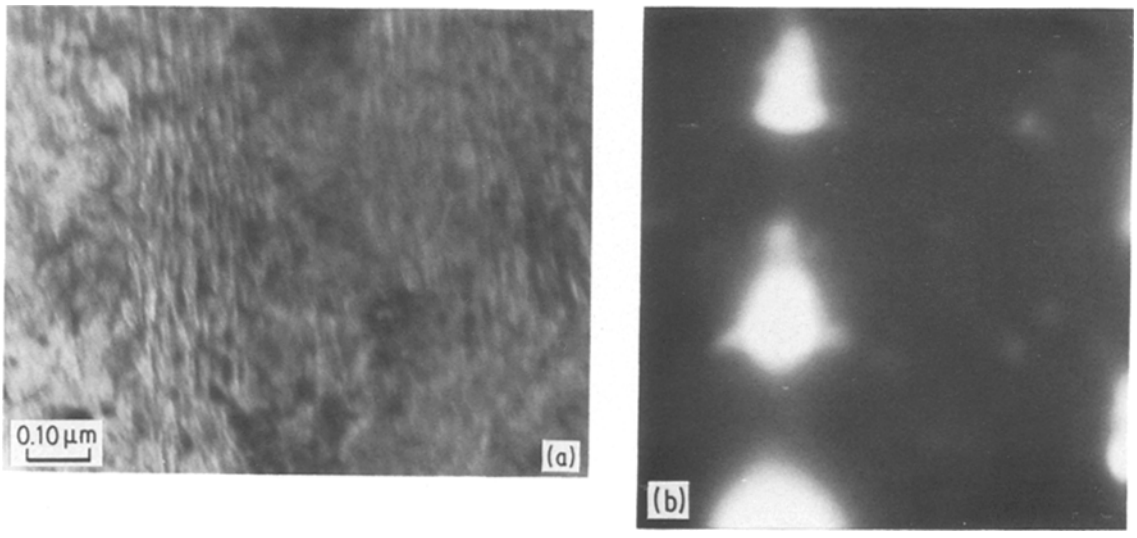

Figure 13 (a) Bright-field image of nitrided case of 321 steel after ion nitriding at 600° C for 10 h and (b) the selected-area diffraction pattern of the corresponding area.

very small platelets on {0 0 1} matrix planes. These precipitates occur in a striated morphology which is apparently the result of strain within the matrix.

References

1. "Metals Handbook", Vol. 4, Heat Treating, 9th Edn (American Society of Metals, Metals Park, Ohio, 1981) p. 191.
2. B. EDENHOFER, *Metall. Mater. Technol.* **8** (1976) 421.
3. *Idem*, *Met. Prog.* **109**(3) (1976) 38.
4. W. D. SOCCORSCY and W. T. EBIHARA, Technical Report, RE 70-156 (Science and Technology Laboratory, Rock Island, Illinois, 1976).
5. P. C. JINDAL, *J. Vac. Sci. Technol.* **15** (1978) 313.
6. R. M. LERNER, *J. Iron Steel Inst. London* **210** (1972) 631.
7. B. EDENHOFER and T. J. BEWLEY, "Heat Treatment '76", edited by P. M. Unterweiser (American Society of Metals, Metals Park, Ohio, 1977) p. 7.
8. V. A. PHILIPHS and A. U. SEYBOLT, *TMS–AIME* **242** (1968) 2415.
9. O. T. INAL and C. V. ROBINO, *Thin Solid Films* **95** (1982) 195.
10. C. V. ROBINO and O. T. INAL, *Mater. Sci. Eng.* **59** (1982) 79.
11. K. OZBAYSAL, O. T. INAL and A. D. ROMIG Jr, *ibid.* **78** (1986) 179.
12. "Metals Handbook", Vol. 7, 8th Edn (American Society of Metals, Metals Park, Ohio, 1972) p. 141.
13. P. GRIEVESON and E. T. TURKDOGAN, *TMS–AIME* **230** (1964) 1604.
14. J. W. CHRISTIAN, "Phase Transformations in Metals and Alloys" (Pergamon, Oxford, 1975) Ch. 9, pp. 411–16.
15. K. SCHWERDFEGER, P. GRIEVESON and E. T. TURKDOGAN, *TMS–AIME* **245** (1969) 1604.
16. D. H. JACK, *Acta Metall.* **24** (1976) 137.

Received 1 November 1985
and accepted 14 March 1986